Role of oxygen within end group substituents on film morphology and charge carrier transport in thiophene/phenylene small-molecule semiconductors

Witold Waliszewski,[1] Zachary S. Parr,[2] Agnieszka Michalska,[1] Roman Halaksa,[2] Hanna Zajaczkowska,[1] Piotr Sleczkowski,[1,3] Marios Neophytou,[4] Beata Luszczynska,[1] Paul W. M. Blom,[5] Christian B. Nielsen,[2,*] Tomasz Marszalek,[1,5,*] Wojciech Pisula[1,5,*]

[1] Department of Molecular Physics, Faculty of Chemistry, Lodz University of Technology, Zeromskiego 116, 90-924 Lodz, Poland
[2] Department of Chemistry, Queen Mary University of London, Mile End Road, London E1 4NS, UK
[3] International Center for Research on Innovative Biobased Materials (ICRI-BioM) - International Research Agenda, Lodz University of Technology, Zeromskiego 116, 90-924 Lodz, Poland
[4] King Abdullah University of Science and Technology (KAUST) KAUST Solar Center (KSC), Thuwal 23955, Saudi Arabia
[5] Max Planck Institute for Polymer Research, Ackermannweg 10, 55128 Mainz, Germany

* Corresponding authors: c.b.nielsen@qmul.ac.uk, marszalek@mpip-mainz.mpg.de, pisula@mpip-mainz.mpg.de

Abstract

In this study, the end group polarity of (5,5')-biphenyl-(2,2')-bithiophenes (PTTPs) was systematically varied from alkyl (**1**) to alkoxy (**2**) with one oxygen atom to glycol (**3**) with two oxygen atoms while the overall length of the end groups is kept constant. Thin films of the three compounds were sublimated at different substrate temperatures and their morphology, crystallinity and charge carrier transport in field-effect transistors was investigated to draw structure-property relationships for the PTTP derivatives. For all three compounds, the effective charge carrier mobility is improved with higher substrate temperatures at which films with higher crystallinity and larger grains are formed. The effective mobility decreases with higher polarity of the end groups from alkyl to alkoxy and glycol. The reliability factor of the alkyl (**1**) and alkoxy (**2**) substituted PTTPs decreases with higher substrate temperature, but at the same

time this value is enhanced for the glycol substituted molecules (**3**). The transistors of **3** prepared at higher substrate temperatures also show a reduced threshold voltage and smaller hysteresis in the transfer characteristics. These insights are important for the understanding of the impact of oxygen incorporation into side chain/end group substituents of organic semiconductors and their implementation in organic electrochemical transistors, thermoelectrics and photovoltaics.

Introduction

Organic semiconductor (OSC) based electronics offer a set of advantages over their inorganic counterparts such as mechanical flexibility, low temperature, and large-area fabrication by solution processing methods. A wide array of devices based on OSCs has been developed such as light-emitting diodes, photovoltaics, memory devices and organic field-effect transistors (OFETs). The performance of the devices can be improved by synthesis of new semiconducting compounds but also by improving and developing novel device architectures, film processing and post-processing techniques [1].

Small-molecule organic semiconductors are widely studied and offer a range of advantages over their high-molecular weight polymer counterparts [2–5]. Because small molecules are characterized by a precise low molecular weight, they can more easily form uniform, ordered structures which are a key factor for charge transport properties in OFETs. Moreover, they are known for their facile purification and ease of processing. Additionally, their relatively simple structure and low molecular weight enable use of vacuum deposition methods to form crystalline and polycrystalline films exhibiting high charge carrier mobilities in OFETs [6]. A promising class of small molecule OSCs are phenylene/thiophene based compounds of varying compositions and lengths that can be easily derivatized with end group substituents to enable

solution processing [7–11]. This class of compounds plays an important role in development of organic electronics since the earliest discoveries of electrical conductivity in organic semiconductors [12,13].

Thiophene-based molecular semiconductors usually afford polycrystalline films with the majority of the molecules oriented with their long axis perpendicular to the substrate surface [14]. These compounds exhibit p-type transport, with mobilities strictly dependent on the material purity and film morphology. Thiophene-based semiconductors display charge carrier mobility as high as 1 $cm^2\ V^{-1}s^{-1}$, but due to their limited solubility, they require vacuum deposition to obtain thin films [15]. It is possible to modify their properties by attaching alkyl side chains and/or end groups to the molecular core to increase the resistance to oxidation, improve crystallinity and solubility while maintaining relatively high charge carrier mobility. Compounds in which both thiophene (T) and phenylene (P) units are incorporated combine excellent electronic and optical properties [16–19]. Therefore, thiophene/phenylene based small molecules with different T:P ratios are widely discussed as prospective organic semiconductors in OFETs.

Thiophene/phenylene-based semiconductors show strong structure-property relationships. In general, the side-chain engineering has a crucial role in improving solubility, processability and electrical properties of the compounds. Side chains are critical for the self-assembly of the semiconductor molecules into distinct supramolecular structures. Usually, linear alkyl chains favor the formation of well-defined layered structures and increase crystallinity, which promotes charge carrier transport. The configuration and chemical structure of the substituents also affect the thermal and thermotropic properties of these OSCs. For instance, long linear alkyl chains yield a broad liquid crystalline phase at low temperatures. Introduction of heteroatoms in the aliphatic chains results in a decrease of the melting temperature [20]. The core planarity of nonbenzofused systems can be improved by weak intramolecular S···O

coupling between an alkoxy group and a sulfur-containing heterocycle such as thiophene leading to a solid-state “conformational lock”[21]. Similar effects on molecular planarity and crystallinity were reported for thio- and seleno-alkyl substitutions [22,23]. Furthermore, branching of the side chains reduces the width of the liquid crystalline phase and decreases the melting temperature [17,24,25].

The incorporation of heteroatoms into the aliphatic end groups of thiophene/phenylene-based OSCs and related fused structures has been explored successfully for transistor-based sensing applications [26–29]. In this work, the influence of oxygen within end group substituents of thiophene/phenylene-based semiconductors on thin film morphology and OFET performance is investigated. The end groups are varied in a systematic manner between alkyl, alkoxy and glycol of same length to determine their role on the final electrical parameters of the device. For studying the end groups and related structure-property relationships, the (5,5’)-biphenyl-(2,2’)-bithiophene (PTTP) core was chosen among the phenylene/thiophene OSCs due to its good charge carrier mobility.

Experimental

1-Bromo-4-hexyl-benzene and 1-bromo-4-pentyloxybenzene were purchased from Tokyo Chemical Industry UK (TCI) and Sigma Aldrich, respectively. The synthesis of 1-bromo-4-(2-ethoxyethoxy)benzene is described in the Supporting Information.

Thermogravimetric analysis (TGA) was carried out on a Mettler 500 at a heating rate of 10 °C/min under nitrogen flow. Differential scanning calorimetry (DSC) was performed on a Mettler DSC 30 at a heating/cooling rate of 10 °C/min under nitrogen flow.

Solution cyclic voltammetry (CV) was performed in dichloromethane solution (0.001 M) with TBAPF6 (0.1 M) as the supporting elecrolyte. The experiments were carried out using a PalmSens 3 electrochemical cell on glassy carbon electrode with Ag/Ag^+ reference electrode

and platinum wire counter electrode. The ionization potentials (IP) were calculated using the formula IP = 4.8 – Ferrocene $E_{1/2}$ + E_{onset}.

Veeco Dimension 3100 Atomic Force Microscope (AFM) was used to inspect the microstructure and the thickness of the sublimed films. All images were obtained in the tapping mode with Olympus silicon cantilevers at 320 kHz resonance frequency. Film thickness analysis was performed by extracting profile of the grains in the height mode with Gwyddion 2.56 software.

To investigate the molecular ordering in the sublimed films, grazing-incidence wide-angle X-ray scattering (GIWAXS) measurements were performed at DELTA (TU Dortmund Synchrotron Electron Accelerator) using beamline BL09 with a photon energy of 10 keV (λ=1.54 Å). The beam size was 1.0mm×0.2mm (width × height), and samples were irradiated below the critical angle for total reflection with respect to the incoming X-ray beam (~0.1°). The scattering intensity was detected on a 2-D image plate (MAR-345) with a pixel size of 150 μm (2300×2300 pixels), and the detector was placed 381 mm from the sample center. The raw detector image had to be converted into reciprocal-space. This was done by using a calibration standard (silver behenate), which has rings at known 2Θ positions. Scattering data is expressed as a function of the scattering vector: $q=4\pi/\lambda \sin(\Theta)$, where Θ is half the scattering angle and λ=1.239 Å is the wavelength of the incident radiation. Here q_{xy} (q_z) is a component of the scattering vector in-plane (out-of-plane) to the sample surface. All X-ray scattering measurements were performed under vacuum (~1 mbar) to reduce air scattering and beam damage of the sample. All GIWAXS data processing and analysis was performed by using the software package Datasqueeze (http://www.datasqueezesoftware.com).

Photoelectron spectroscopy in air (PESA) was employed to determine the ionization potential of the materials. The measurements were performed at room temperature with a Riken Keiki spectrometer (Model AC-2) and the samples were coated on glass substrates.

Field-effect transistors were fabricated in a top-contact, bottom-gate configuration. As substrates, highly doped silicon (Si) wafers with a 300 nm thick thermally grown silicon oxide (SiO_2) layer were used. Before OSC film deposition the Si/SiO_2 substrates were ultrasonically cleaned in acetone and isopropanol, then treated with a freshly prepared piranha solution ($7H_2SO_4$:$3H_2O_2$) at 90 °C for 60 minutes to remove trace amounts of organic residues from the surface. Next, the Si/SiO_2 wafers were rinsed few times using methanol and deionized water and dried with nitrogen gas. Subsequently, the substrate surface was modified with octadecyltrichlorosilane (OTS). OTS silanization was performed by immersing the cleaned silicon wafers into a 0.5% solution of OTS in chloroform and hexane [1:40:160] for 30 minutes. After this process, the substrates were rinsed three times with chloroform for 10 minutes each and dried again with nitrogen gas. The purpose of the OTS treatment was the creation of a self-assembled monolayer (SAM), which reduces the surface energy of the inorganic dielectric and ensures a three-dimensional growth of the organic film.

Thermal evaporation of the PTTP compounds was performed below 10^{-5} mbar at rate 0.05-0.1 Å/s and various substrate temperatures using a TecTra Mini-Coater high vacuum coating system. The film thickness was about 50 nm controlled using a quartz crystal microbalance monitor and measured by atomic force microscopy. The substrate temperatures were chosen based on the DSC and TGA results for each compound. In the last step of the OFET fabrication, 50 nm thick source and drain electrodes were deposited on the organic film by evaporating gold via shadow masks at a rate of 1 Å/s. Channel lengths of 30 μm, 40 μm, 50 μm, 60 μm, and 80 μm and channel width of 1 mm were applied. The transistor characterization was performed in nitrogen atmosphere using a Keithley 4200 semiconductor system. Drain-source current (I_{DS})

was measured at gate-source voltage (V_{GS}) sweeps from +10 to -80 V at constant drain-source voltage (V_{DS}) of -40 V. The charge carrier mobilities were deduced from the transfer characteristics in the saturation regime using equation:

$$I_{DS} = \frac{W}{2L} C_i \mu (V_G - V_{TH})^2,$$

where I_{DS} is the drain current, W the channel width, L the channel length, C_i the capacitance of gate dielectric, V_G the gate voltage and V_{TH} the threshold voltage. The reported mobilities are averaged values over eight transistors.

Results and discussion

The PTTP compounds studied in this work, 5,5′-bis(4-*n*-hexylphenyl)-2,2′-bithiophene (**1**), 5,5′-bis(4-(*n*-pentyloxy)phenyl)-2,2′-bithiophene (**2**) and 5,5′-bis(4-(2-ethoxyethoxy)phenyl)-2,2′-bithiophene (**3**), were synthesized following the route depicted in Scheme 1 and briefly outlined here. Using an established literature procedure [27], a Pd-catalyzed Stille coupling reaction between 5,5'-bis(trimethylstannyl)-2,2'-bithiophene and 1-bromo-4-hexylbenzene afforded **1** as a yellow powder in 75% yield. 1-Bromo-4-pentyloxybenzene and 1-bromo-4-(2-ethoxyethoxy)benzene were similarly reacted under Stille conditions with 5,5'-bis(trimethylstannyl)-2,2'-bithiophene to afford final compounds **2** (yellow powder, 80% yield) and **3** (orange powder, 75% yield). All synthesis details can be found in the supporting information.

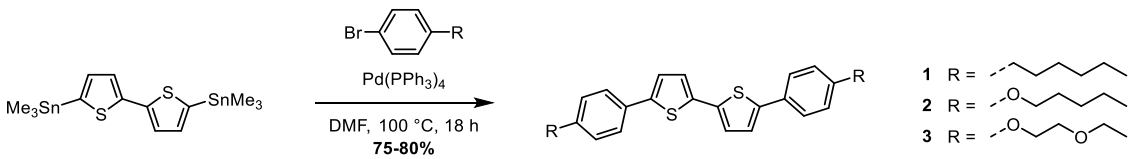

Scheme 1. Synthesis of 5,5′-bis(4-*n*-hexylphenyl)-2,2′-bithiophene (**1**), 5,5′-bis(4-(*n*-pentyloxy)phenyl)-2,2′-bithiophene (**2**) and 5,5′-bis(4-(2-ethoxyethoxy)phenyl)-2,2′-bithiophene (**3**).

Cyclic voltammetry (CV) of the three compounds was performed in solution to investigate the intrinsic ionization potentials eliminating any solid-state effects (Figure S1). This afforded IP values of 5.27 eV for **1**, 5.13 eV for **2** and 5.14 eV for **3**. This trend can be explained by the electron-donating oxygen atoms (resonance effect from the oxygen lone pairs) attached directly to the PTTP chromophore in **2** and **3**. The density functional theory calculations performed for the three PTTP compounds are in good agreement with the experimental data (Figure S2).

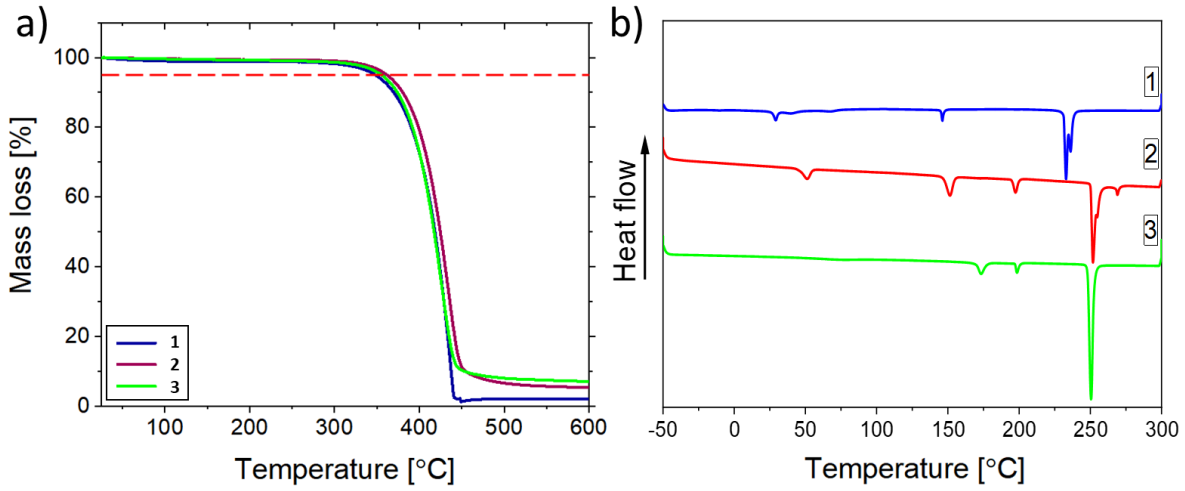

Figure 2. a) Thermogravimetry and b) second heating differential scanning calorimetry curves of compounds **1**, **2**, **3**. 5% mass loss of compounds visible in the TGA graph as a red dashed line.

In order to investigate the effect of the different end groups on the thermal properties of the PTTPs, an analysis of differential scanning calorimetry (DSC) and thermogravimetry (TGA) scans was performed. The TGA curves in Figure 2a show that 5% mass loss of the compounds **1**, **2**, and **3** is observed at 332 °C, 348 °C and 338 °C, respectively. Values of the inflection points at the derivative thermogravimetry (Figure S3) curves for all compounds were observed at around 430 °C (435 °C, 434 °C and 426 °C for **1**, **2**, and **3**, respectively). The incorporation of oxygen atoms in the end groups of **2** and **3** reduces their thermal decomposition in

comparison to **1**. Presence and the position of oxygen in the side chain was reported as having influence on the thermal properties of the compounds [30,31]. The more complete decomposition of **1** is also evident at the high temperature of 435 °C at which this compound shows the highest weight loss of 90% in comparison to **2** and **3** with 90% decomposition at 450 °C. In case of **1**, the final mass loss is around 1% as opposed to **2** and **3** (with 6% and 8% residual mass, respectively) which implies that the degradation mechanism of the alkyl side chains involves the release of more volatile components.

The DSC scans in Figure 2b exhibit thermal phase transitions for the PTTPs in the temperature range from -50 °C to 300 °C. The melting point is represented by the sharp endothermic peak at 233 °C, 252 °C and 250 °C for **1**, **2** and **3**, respectively. The melting point of alkyl-substituted **1** is lower than in the case of alkoxy- and glycol-substituted **2** and **3**, whose melting points appear nearly at the same temperature. The higher melting temperature corresponds to the more pronounced thermal stability observed in the TGA scans. As all side chains have the same length, the difference in the thermal transition temperatures is certainly caused by the presence of oxygen atoms in **2** and **3**. The observed thermal properties based on TGA and DSC study of compounds **1** and **2** are in line with the results reported in the literature [9,11]. For **1**, two crystalline phase transitions are observed at 29 °C and 146 °C. For **2**, three crystalline phase transitions appear at 23 °C, 104 °C and 163 °C, whereas **3** displays transitions at 162 °C and 191 °C**.** The substrate temperatures for subsequent sublimation of the compounds (vide infra) were chosen based on the DSC data as summarized in Figure 3. Since the first phase transition of **3** is observed for a higher temperature (173 °C) only three substrate temperatures were chosen for this compound. For compounds **1** and **2** four substrate temperatures were selected. For all investigated compounds, the lowest temperature was 25 °C and the highest was 180 °C, which is significantly lower than the melting point of each compound.

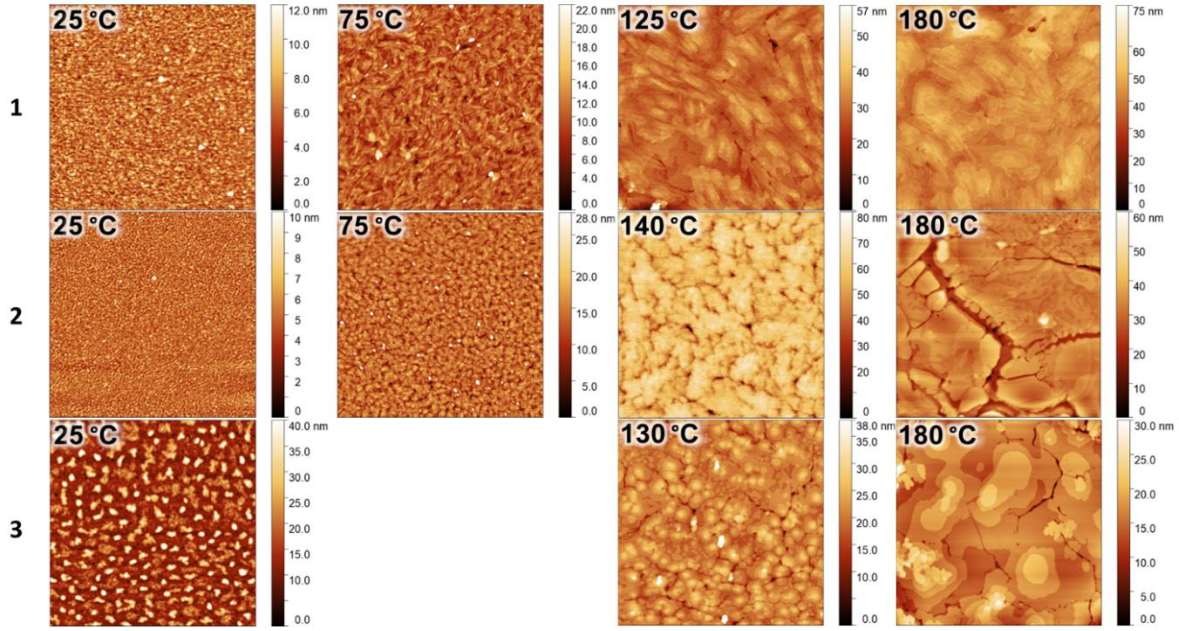

Figure 3. AFM height images (15 µm × 15 µm) of PTTP derivatives **1**-**3** as thin films deposited by vacuum deposition onto OTS-modified Si/SiO_2 wafers at various temperatures.

The 50 nm thick PTTP films were thermally evaporated on piranha-treated and OTS-modified Si/SiO_2 wafers at various substrate temperatures. The reason for thermal evaporation was the rather low solubility of these compounds on the order of 2 mg/ml, which makes it difficult to obtain good-quality thin films by solution deposition techniques. Thermal evaporation provides an excellent way to well control the growth of homogenous films. Previous studies of phenylene-thiophene based small-molecule materials for OFET applications consistently across several derivatives show that evaporated OFET devices perform better than solution-processed ones [9]. Atomic force microscopy (AFM) was subsequently used to investigate the influence of the deposition temperatures on the film morphologies of the PTTP derivatives. The same substrates and deposition conditions were used for the OFET fabrication discussed below. The AFM images in Figure 3 display significant differences in the film microstructure between **1**, **2** and **3**. For films deposited at 25 °C the morphology differs only slightly. All three compounds

show randomly distributed small grains, whereby the grain size increases with the number of oxygen atoms in the side chain from 0.3 µm for **1** to 0.8 µm for **3**. At higher sublimation temperature of 75 °C, the grains for **1** and **2** become to some extent larger, and in the case of **1** change to a fibrous texture. With a further substrate temperature rise during deposition to 125 °C and 180 °C, much larger grains as flat islands are formed for the three compounds suggesting a gradual film growth. The height profile for **3** discloses a step-terrace structure (Figure S4), which is characteristic for a layer-plus island Stranski−Krastanov (SK) growth [32]. Interestingly, while the RMS roughness for films of **1** and **2** increases with higher substrate temperature during thermal evaporation, the roughness for **3** is reduced, as summarized in Table S1, resulting in the most distinct step-terrace film morphology. This is a similar initial growth pattern, as reported for pentacene [33] and C8-BTBT [34]. In this growth model, the molecules approaching the substrate are more bound to the substrate than to each other. This causes the first molecules to condense into a highly ordered monolayer on the surface. Flat islands are then formed on the initial layer, with a height of 2.5 nm corresponding to the interplanar spacing of the compounds as determined by GIWAXS. During the SK growth, the flat islands grow laterally to eventually merge into a continuous layer, which can be partially observed for **3** at the substrate temperature of 130 °C and 180 °C. However, the films of **2** and **3** deposited at 180 °C exhibit serious cracks on the surface spanning over the whole AFM images with depths of at least 40 nm. The crack formation in the thin films can be attributed to a mismatch of the thermal expansion coefficient between the organic layer of **2** and **3** and the inorganic silicon substrate [9,17,25,35]. The discrepancy in the coefficient induces high stress during cooling down from the high substrate temperature followed by fractures in the organic film. This phenomenon is described as “misfit strain” in layered systems [33]. It should be noted that only compounds **2** and **3** show cracking, which is attributed to the presence of oxygen atoms in the end groups. The alkoxy and glycol chains possess higher spatial freedom in comparison to alkyl

substituents increasing the mismatch to the silicon substrate [9,17,35]. The morphology study discloses a considerable role of the substrate temperature on the microstructure of the sublimated films. For the three PTTPs, a similar trend is found where larger grains are formed at higher temperatures which is expected to favor the charge carrier transport in OFETs.

The molecular organization of the PTTPs was investigated using grazing incidence wide-angle X-ray scattering (GIWAXS). All three compounds show an edge-on molecular arrangement on the surface as implied by the corresponding GIWAXS patterns in Figure 4. The out-of-plane reflections confirm a layered structure oriented parallel to the substrate with an interlayer spacing of 29.9 Å for **1**, in agreement with [36], 28.9 Å for **2** and 27.7 Å for **3** in films deposited at 25 °C. The interlayer distances were determined from the main 100 reflections observed at q_z = 0.210 Å^{-1}, q_z = 0.217 Å^{-1} and q_z = 0.226 Å^{-1}, respectively. The decrease in the spacing observed from **1** to **3** is in agreement with the higher spatial freedom with more oxygen atoms present in the end group. Deposition of the compounds at higher substrate temperature of 180 °C improves the molecular order (Figure 4). Interestingly, the out-of-plane interlayer distance of **1** decreases to 27.3 Å as derived from the main interlayer reflection at q_{xy} = 0 Å^{-1} and q_z =0.228 Å^{-1} (Figure 4b). This decrease could origin from a tighter out-of-plane packing of the molecules due to interdigitation of the end groups and/or stronger tilting of the molecules towards the substrate. In contrast to **1**, the out-of-plane interlayer distance of **2** and **3** remains unchanged at the substrate temperature of 180 °C. For all three compounds, the elevated substrate temperature leads to a large number of new intensive wide-angle reflections indicating higher molecular packing within the layers. Reflections for **1** at d = 3.95 Å and d = 4.72 Å are assigned to the π-stacking and the in-plane layer distance, respectively. These values are in agreement with the ones reported for unsubstituted PTTP [37]. The off-equatorial position of the π-stacking reflection at q_{xy} = 1.575 Å^{-1} and q_z = 0.5 Å^{-1} confirms a ~20° tilting of the main core with respect to the out-of-plane direction. In comparison to **1**, the π-stacking distance of

3.72 Å for **2** and **3** is reduced as the corresponding reflection is located at in-plane q_{xy} = 1.71 Å^{-1} q_z = 0.0 Å^{-1} (Figure 4f) which also suggests no tilting of the main cores towards the surface. In this case, oxygen atoms in the side chains provide higher spatial freedom to the substituents and change the organization of the main core in respect to the surface. The interdigitation of the side chains could be responsible for reduction of the interlayer distance. Besides the determined spacings, also the molecular order is important for the in-plane charge carrier transport in OFETs. As evident from the GIWAXS patterns in Figure 4, compound **1** shows significantly sharper reflections related to the intermolecular packing in the wide-angle region. In contrast, for compound **3** these reflections are much broader and smeared out. indicating a lower degree of order. The difference in order can be related to the flexibility of the various side chains. Less flexible substituents such as the alkyl side chains improve the molecular order of **1**.

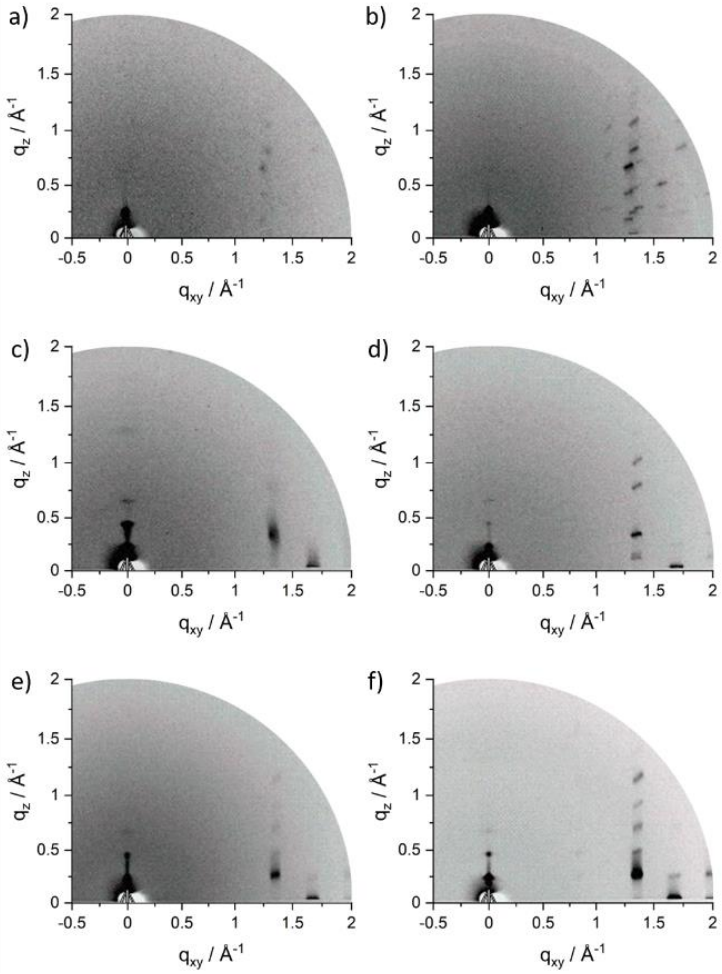

Figure 4. GIWAXS patterns of compound **1** (a, b), **2** (c, d) and **3** (e, f) as thin films deposited at the substrate temperatures of 25 °C (a, c, and e) and 180 °C (b, d, and f).

The ionization potential (IP) of the three sublimed compounds was determined by photoelectron spectroscopy in atmosphere (PESA). The thin films deposited at 25 °C reveal IP values of 5.18 eV for **1**, 5.15 eV for **2** and 4.85 eV for **3** indicating a decrease of the highest occupied molecular orbital (HOMO) energy level with larger number of oxygen atoms in the end groups (Figure S5). In comparison to the CV data for solution, the PESA results indicate a smaller IP for **3** compared to **2** in the solid state. We ascribe this to the solid-state effect. Taking into consideration the fact that these molecules orient with their long axis perpendicular to the substrate, we can infer that the peripheral solubilizing chains will predominantly face towards the surface of the film. The more electron-rich ethylene glycol chain in compound **3** will thus decrease the IP as for instance also seen in the case of electron-donating self-assembled monolayers used to decrease the work function of metal electrodes.

The alignment of the HOMO energy level of the organic semiconductor with the work function of around 4.9 eV for the Au electrodes can effectively lower the injection barrier for hole carriers and in this way improve the reliability of the OFET devices. To determine the influence of the end groups on the charge carrier transport of the PTTP derivatives, top-contact, bottom-gate OFETs were fabricated. Transfer characteristics were obtained for V_{GS} sweeps from +10 V to –40 V at constant V_{DS} of –40 V and are presented in Figure 5. The charge carrier mobilities were calculated from the saturation regime. All OFETs reveal typical p-channel behavior and the operation parameters are summarized in Table S2. To take into account the double-slope character of the curves and to assess realistic device parameters, the reliability factor and the corresponding effective charge carrier mobility were determined [38,39]. Interestingly, the reliability factor decreases for **1** and **2** with higher substrate temperature, while the factor

significantly improves for **3** (Figure 6a). Although the reliability factor decreases, the effective charge carrier mobility of **1** increases from $4.8 \cdot 10^{-2}$ $cm^2V^{-1}s^{-1}$ for films deposited at 25 °C to $4.3 \cdot 10^{-1}$ $cm^2V^{-1}s^{-1}$ for 125 °C and $1.3 \cdot 10^{-1}$ $cm^2V^{-1}s^{-1}$ for 180 °C remaining the highest value along the three studied PTTPs (Figure 5a). The higher performance of **1** at all substrate temperatures is attributed to the higher molecular order as assigned in the GIWAXS study (Figure 4). Despite the larger π-stacking distance of **1** in comparison to **2** and **3**, the improved molecular order particularly favors the in-plane charge carrier transport in the OFET device. The threshold voltage was derived from the original transfer characteristics and changes from 7 V for the deposition temperature of 25 °C to -15 V for 180 °C. The effective charge carrier mobility of **2** also increases with higher substrate temperature from $9.5 \cdot 10^{-3}$ $cm^2V^{-1}s^{-1}$ for films deposited at 25 °C to $6.5 \cdot 10^{-2}$ $cm^2V^{-1}s^{-1}$ for 180 °C but remains lower in comparison to **1**. The threshold voltage of **2** also increases from -7 V to -15 V (Figure 6c). The strongest rise in the effective charge carrier mobility is observed for **3**. The mobility increases from $2.0 \cdot 10^{-5}$ $cm^2V^{-1}s^{-1}$ for films deposited at 25 °C to $2.5 \cdot 10^{-2}$ $cm^2V^{-1}s^{-1}$ for the substrate temperature of 180 °C. In contrast to **1** and **2**, the threshold voltage significantly improves from -20 V to only -3 V (Figure 6c) resulting in the enhanced reliability factor. The on/off current ratio equal of around 10^5-10^6 is comparable to values found for all three compounds.

A close correlation between the substrate temperature, the effective charge carrier mobility and film morphology is found. For all the studied compounds, the effective mobility increases with higher substrate temperature during film deposition at which larger grains are grown. The large-grain morphology and higher film crystallinity result in mobility values higher by at least an order of magnitude in comparison to films obtained at low substrate temperature. The improved device performance can be rationalized by smaller amount of grain boundaries, which typically reduce the long-range charge transport by creating charge carrier traps.

The beneficial impact of the elevated substrate temperature on the OFET performance is further manifested by the lower contact resistance R_c. The analysis of OFETs comprising thin films of **3** by the transfer line method (TLM) reveals a significant decrease of R_c for films deposited at higher temperatures [40]. In particular, OFETs comprising thin films deposited on substrates at 130 °C and 180 °C exhibit R_c of $4.1 \cdot 10^4$ Ohm · cm and $4.6 \cdot 10^4$ Ohm · cm, respectively, that are smaller by more than two orders of magnitude in comparison to $2.4 \cdot 10^7$ Ohm · cm for devices prepared at 25 °C (Figure S6). Since large values of R_c are normally ascribed to the notable injection barrier for the charge injection from the electrode to the organic semiconductor, the lower R_c implies a more efficient charge injection for films of **3** deposited at substrates at 130 °C and 180 °C. The improved OSC/electrode interface of **3** is not only reflected by the diminished R_c, but also originates from the growth of larger grains. Additionally, the low resistance for **3** is favored by a match between the ionization potential of 4.85 eV for the compound, that can be approximated as its HOMO energy level, and the work function of around 4.9 eV for Au reducing the injection barrier for holes. Both factors lead to the enhanced overall transistor performance for films prepared at higher substrate temperature as also expressed by the higher reliability factor and a smaller hysteresis in the transfer plots for **3** in comparison to **1** and **2**.

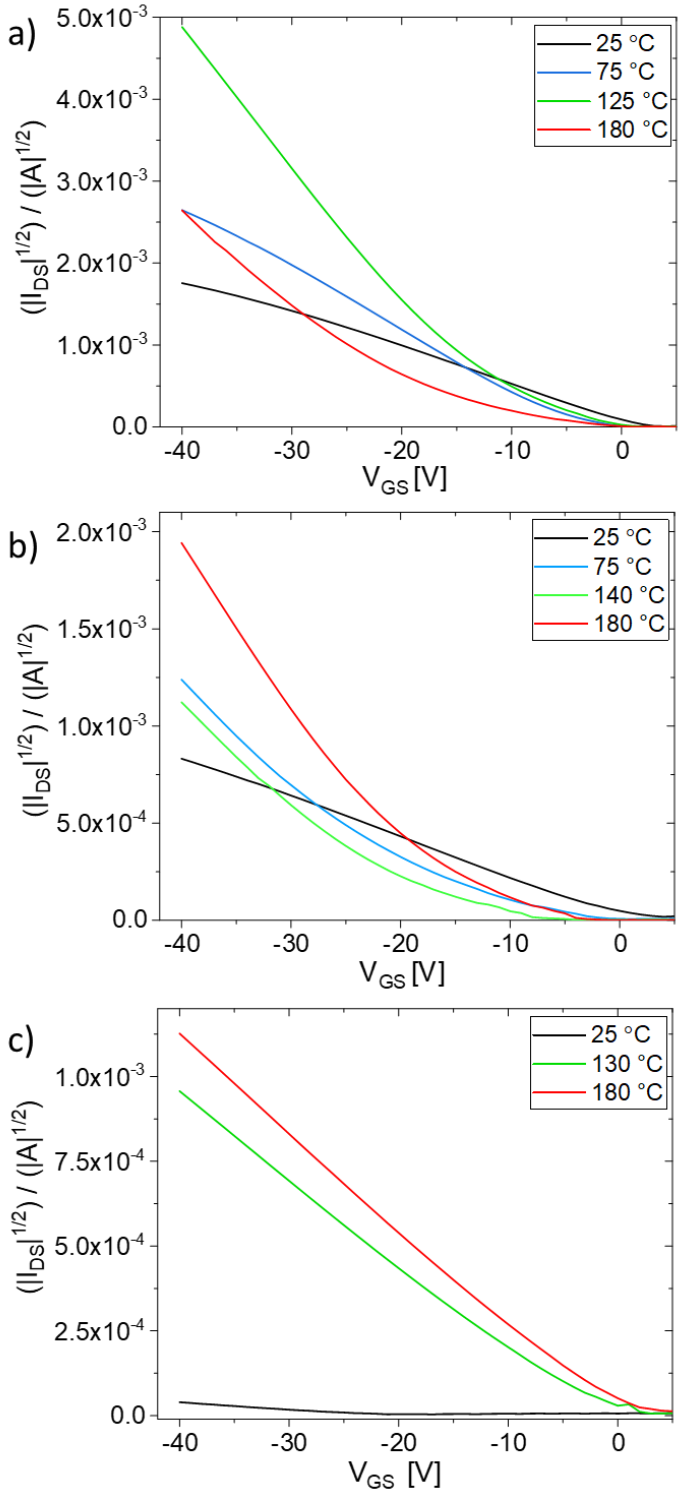

Figure 5. Transfer characteristics shown as a square root of I_{DS} at V_{DS} = -40 V for the PTTP derivatives a) **1**, b) **2**, and c) **3** deposited at various temperatures.

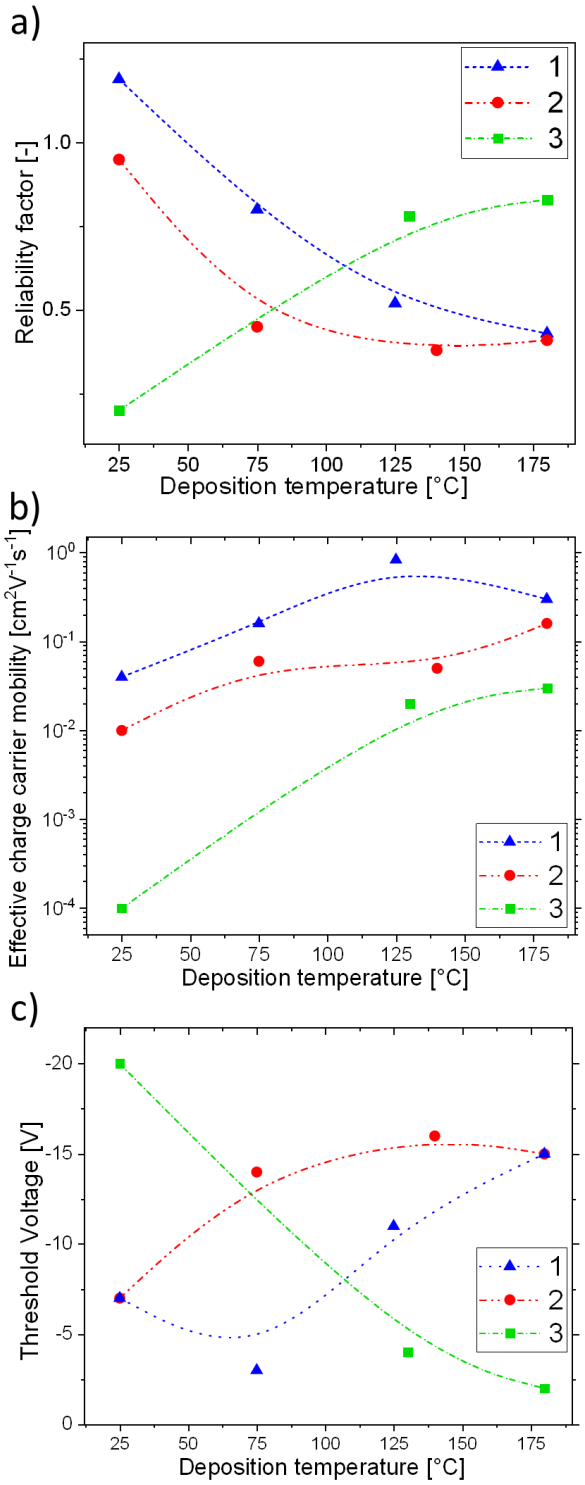

Figure 6. Influence of substrate temperature during deposition in field effect transistors with **1**, **2** and **3** based active channels on a) reliability factor, b) effective charge mobility and c) threshold voltage. Lines are eye guides.

Conclusions

In this work, the influence of end group substituents on surface morphology, microstructure and charge carrier transport in thin films of thiophene/phenylene based small-molecule semiconductors was investigated, in particular focusing on the PTTP model system. Three PTTP derivatives with varying degree of end group polarity have been analysed as potential active materials in organic field-effect transistors. More specifically, the end group polarity was altered by going from an alkyl derivative of PTTP (**1**) to an alkoxy derivative (**2**) with one oxygen atom in each end group to the glycol derivative (**3**) with two oxygen atoms in each end group while maintaining the overall length of the end groups constant across the three compounds. For all three derivatives, the effective charge carrier mobility increases with higher substrate temperature during sublimation that is related to growth of larger grains and higher film crystallinity. Furthermore, it is observed that the mobility decreases with higher polarity of the end groups, but at the same time the reliability of the devices significantly improves. While the reliability factor decreases for **1** and **2** with higher substrate temperature, this value is enhanced for **3**. This is in agreement with the reduced threshold voltage and smaller hysteresis during device operation of **3**. These results provide fundamental understanding on the role of oxygen incorporation into semiconductor side chain/end group substituents as this approach has seen rapidly growing attention in recent years in the organic electronics community, not only for OFET and organic electrochemical transistor (OECT) applications, but also for organic thermoelectric and photovoltaic applications [41–47].

Acknowledgments

W. Waliszewski and W. Pisula acknowledge the National Science Centre, Poland through the grant UMO-2019/33/B/ST3/1550. A Michalska, H. Zajaczkowska, P. Sleczkowski, B. Luszczynska, T. Marszalek and W. Pisula acknowledge the Foundation for Polish Science financed by the European Union under the European Regional Development Fund (POIR.04.04.00-00-3ED8/17). Z. S. Parr and C. B. Nielsen acknowledge support from the Academy of Medical Sciences & Wellcome Trust (SBF002/1158). The authors also acknowledge Beamline 9 of the DELTA electron storage ring in Dortmund for providing synchrotron radiation and technical support for GIWAXS measurements.

Bibliography:

[1] J. Mei, Y. Diao, A.L. Appleton, L. Fang, Z. Bao, Integrated materials design of organic semiconductors for field-effect transistors, J. Am. Chem. Soc. 135 (2013) 6724–6746. https://doi.org/10.1021/ja400881n.

[2] M.M. Torrent, C. Rovira, Novel small molecules for organic field-effect transistors: Towards processability and high performancens, Chem. Soc. Rev. 37 (2008) 827–838. https://doi.org/10.1039/b614393h.

[3] H. Yamada, T. Okujima, N. Ono, Organic semiconductors based on small molecules with thermally or photochemically removable groups, Chem. Commun. (2008) 2957–2974. https://doi.org/10.1039/b719964c.

[4] J.F. Chang, W.R. Chen, S.M. Huang, Y.C. Lai, X.Y. Lai, Y.W. Yang, C.H. Wang, High mobility ambipolar organic field-effect transistors with a nonplanar heterojunction structure, Org. Electron. Physics, Mater. Appl. 27 (2015) 84–91. https://doi.org/10.1016/j.orgel.2015.09.008.

[5] Q. Meng, W. Hu, Recent progress of n-type organic semiconducting small molecules for organic field-effect transistors, Phys. Chem. Chem. Phys. 14 (2012) 14152. https://doi.org/10.1039/c2cp41664f.

[6] L. Lyu, D. Niu, H. Xie, Y. Zhao, N. Cao, H. Zhang, Y. Zhang, P. Liu, Y. Gao, The correlations of the electronic structure and film growth of 2,7-diocty[1]benzothieno[3,2-b]benzothiophene (C8-BTBT) on SiO 2, Phys. Chem. Chem. Phys. 19 (2017) 1669–1676. https://doi.org/10.1039/C6CP06919C.

[7] S. Hotta, K. Waragai, Alkyl-substituted oligothiophenes: Crystallographic and

spectroscopic studies of neutral and doped form, J. Mater. Chem. 1 (1991) 835–842. https://doi.org/10.1039/jm9910100835.

[8] A.L. Deman, J. Tardy, Y. Nicolas, P. Blanchard, J. Roncali, Structural effects on the characteristics of organic field effect transistors based on new oligothiophene derivatives, Synth. Met. 146 (2004) 365–371. https://doi.org/10.1016/j.synthmet.2004.08.015.

[9] M. Mushrush, A. Facchetti, M. Lefenfeld, H.E. Katz, T.J. Marks, Easily Processable Phenylene−Thiophene-Based Organic Field-Effect Transistors and Solution-Fabricated Nonvolatile Transistor Memory Elements, J. Am. Chem. Soc. 125 (2003) 9414–9423. https://doi.org/10.1021/ja035143a.

[10] Q. Yuan, S.C.B. Mannsfeld, M.L. Tang, M.F. Toney, J. Lüning, Z. Bao, Thin film structure of tetraceno[2,3-b]thiophene characterized by grazing incidence X-ray scattering and near-edge X-ray absorption fine structure analysis, J. Am. Chem. Soc. 130 (2008) 3502–3508. https://doi.org/10.1021/ja0773002.

[11] A. Sung, M.M. Ling, M.L. Tang, Z. Bao, J. Locklin, Correlating molecular structure to field-effect mobility: The investigation of side-chain functionality in phenylene-thiophene oligomers and their application in field effect transistors, Chem. Mater. 19 (2007) 2342–2351. https://doi.org/10.1021/cm070117n.

[12] F. Garnier, A. Yassar, R. Hajlaoui, G. Horowitz, F. Deloffre, B. Servet, S. Ries, P. Alnot, Molecular Engineering of Organic Semiconductors: Design of Self-Assembly Properties in Conjugated Thiophene Oligomers, J. Am. Chem. Soc. 115 (1993) 8716–8721. https://doi.org/10.1021/ja00072a026.

[13] J. ping Zhou, M. Dong, Y. Nio, F. min Kong, X. yu Zheng, K. jian Guo, H. Meng, Z. Bao, A.J. Lovinger, B.C. Wang, A.M. Mujsce, High field-effect mobility oligofluorene

derivatives with high environmental stability [1], J. Am. Chem. Soc. 123 (2001) 9214–9215. https://doi.org/10.1021/ja016525o.

[14] A. Mishra, C.Q. Ma, P. Bäuerle, Functional oligothiophenes: Molecular design for multidimensional nanoarchitectures and their applications, Chem. Rev. 109 (2009) 1141–1176. https://doi.org/10.1021/cr8004229.

[15] F.A. Larik, M. Faisal, A. Saeed, Q. Abbas, M.A. Kazi, N. Abbas, A.A. Thebo, D.M. Khan, P.A. Channar, Thiophene-based molecular and polymeric semiconductors for organic field effect transistors and organic thin film transistors, Springer US, 2018. https://doi.org/10.1007/s10854-018-9936-9.

[16] T. Taniguchi, K. Fukui, R. Asahi, Y. Urabe, A. Ikemoto, J. Nakamoto, Y. Inada, T. Yamao, S. Hotta, Enhanced performance of organic solar cells based on thiophene/phenylene co-oligomers, Synth. Met. 227 (2017) 156–162. https://doi.org/10.1016/j.synthmet.2017.04.007.

[17] P.G.A. Janssen, M. Pouderoijen, A.J.J.M. Van Breemen, P.T. Herwig, G. Koeckelberghs, A.R. Popa-Merticaru, S.C.J. Meskers, J.J.P. Valeton, E.W. Meijer, A.P.H.J. Schenning, Synthesis and properties of α,ω-phenyl-capped bithiophene derivatives, J. Mater. Chem. 16 (2006) 4335–4342. https://doi.org/10.1039/b608441a.

[18] S. Hotta, T. Yamao, The thiophene/phenylene co-oligomers: Exotic molecular semiconductors integrating high-performance electronic and optical functionalities, J. Mater. Chem. 21 (2011) 1295–1304. https://doi.org/10.1039/c0jm02290j.

[19] I. Perepichka, D. Perepichka, Handbook of Thiophene-based Materials : Applications in Organic Electronics and Photonics, John Wiley & Sons, Ltd., 2009.

[20] A.A.Y. Guilbert, Z.S. Parr, T. Kreouzis, D.J. Woods, R.S. Sprick, I. Abrahams, C.B.

Nielsen, M. Zbiri, Effect of substituting non-polar chains with polar chains on the structural dynamics of small organic molecule and polymer semiconductors, Phys. Chem. Chem. Phys. 23 (2021) 7462–7471. https://doi.org/10.1039/d1cp00670c.

[21] Y. Liu, Z. Zhang, S. Feng, M. Li, L. Wu, R. Hou, X. Xu, X. Chen, Z. Bo, Exploiting Noncovalently Conformational Locking as a Design Strategy for High Performance Fused-Ring Electron Acceptor Used in Polymer Solar Cells, J. Am. Chem. Soc. 139 (2017) 3356–3359. https://doi.org/10.1021/jacs.7b00566.

[22] S. Vegiraju, B.-C. Chang, P. Priyanka, D.-Y. Huang, K.-Y. Wu, L.-H. Li, W.-C. Chang, Y.-Y. Lai, S.-H. Hong, B.-C. Yu, C.-L. Wang, W.-J. Chang, C.-L. Liu, M.-C. Chen, A. Facchetti, Intramolecular Locked Dithioalkylbithiophene-Based Semiconductors for High-Performance Organic Field-Effect Transistors, Adv. Mater. 29 (2017) 1702414. https://doi.org/10.1002/adma.201702414.

[23] S.N. Afraj, C. Lin, A. Velusamy, C. Cho, H. Liu, J. Chen, G. Lee, J. Fu, J. Ni, S. Tung, S. Yau, C. Liu, M. Chen, A. Facchetti, Heteroalkyl-Substitution in Molecular Organic Semiconductors: Chalcogen Effect on Crystallography, Conformational Lock, and Charge Transport, Adv. Funct. Mater. (2022) 2200880. https://doi.org/10.1002/adfm.202200880.

[24] M. Halik, H. Klauk, U. Zschieschang, G. Schmid, S. Ponomarenko, S. Kirchmeyer, W. Weber, Relationship between molecular structure and electrical performance of oligothiophene organic thin film transistors, Adv. Mater. 15 (2003) 917–922. https://doi.org/10.1002/adma.200304654.

[25] N.L. Campbell, W.L. Duffy, G.I. Thomas, J.H. Wild, S.M. Kelly, K. Bartle, M. O'Neill, V. Minter, R.P. Tuffin, Nematic 2,5-disubstituted thiophenes, J. Mater. Chem. 12 (2002) 2706–2721. https://doi.org/10.1039/b202073b.

[26] J. Huang, J. Miragliotta, A. Becknell, H.E. Katz, Hydroxy-terminated organic semiconductor-based field-effect transistors for phosphonate vapor detection, J. Am. Chem. Soc. 129 (2007) 9366–9376. https://doi.org/10.1021/ja068964z.

[27] Z.S. Parr, R.B. Rashid, B.D. Paulsen, B. Poggi, E. Tan, M. Freeley, M. Palma, I. Abrahams, J. Rivnay, C.B. Nielsen, Semiconducting Small Molecules as Active Materials for p-Type Accumulation Mode Organic Electrochemical Transistors, Adv. Electron. Mater. 6 (2020). https://doi.org/10.1002/aelm.202000215.

[28] C.J. Kousseff, R. Halaksa, Z.S. Parr, C.B. Nielsen, Mixed Ionic and Electronic Conduction in Small-Molecule Semiconductors, Chem. Rev. 122 (2022) 4397–4419. https://doi.org/10.1021/acs.chemrev.1c00314.

[29] N. Turetta, M.A. Stoeckel, R. Furlan De Oliveira, F. Devaux, A. Greco, C. Cendra, S. Gullace, M. Gicevičius, B. Chattopadhyay, J. Liu, G. Schweicher, H. Sirringhaus, A. Salleo, M. Bonn, E.H.G. Backus, Y.H. Geerts, P. Samorì, High-Performance Humidity Sensing in π-Conjugated Molecular Assemblies through the Engineering of Electron/Proton Transport and Device Interfaces, J. Am. Chem. Soc. 144 (2022) 2546–2555. https://doi.org/10.1021/jacs.1c10119.

[30] B.X. Dong, C. Nowak, J.W. Onorato, T. Ma, J. Niklas, O.G. Poluektov, G. Grocke, M.F. Ditusa, F.A. Escobedo, C.K. Luscombe, P.F. Nealey, S.N. Patel, Complex Relationship between Side-Chain Polarity, Conductivity, and Thermal Stability in Molecularly Doped Conjugated Polymers, Chem. Mater. 33 (2021) 741–753. https://doi.org/10.1021/acs.chemmater.0c04153.

[31] D.T. Tran, A. Gumyusenge, X. Luo, M. Roders, Z. Yi, A.L. Ayzner, J. Mei, Effects of Side Chain on High Temperature Operation Stability of Conjugated Polymers, ACS Appl. Polym. Mater. 2 (2020) 91–97. https://doi.org/10.1021/acsapm.9b00999.

[32] A. Baskaran, P. Smereka, Mechanisms of Stranski-Krastanov growth, J. Appl. Phys. 111 (2012). https://doi.org/10.1063/1.3679068.

[33] D.P. Niyamakom, Influence of deposition parameters on morphology , growth and structure of crystalline and amorphous organic thin films, (2008).

[34] Y. Huang, J. Sun, J. Zhang, S. Wang, H. Huang, J. Zhang, D. Yan, Y. Gao, J. Yang, Controllable thin-film morphology and structure for 2,7-dioctyl[1]benzothieno[3,2-b][1]benzothiophene (C8BTBT) based organic field-effect transistors, Org. Electron. 36 (2016) 73–81. https://doi.org/10.1016/j.orgel.2016.05.019.

[35] H. Mochizuki, Y. Kawaguchi, F. Sasaki, M. Chikamatsu, R. Azumi, S. Hotta, Optimization of thermal treatment of vapor-deposited thiophene/phenylene co-oligomer films, J. Cryst. Growth. 345 (2012) 39–43. https://doi.org/10.1016/j.jcrysgro.2012.02.024.

[36] S. Vaidyanathan, F. Dötz, H.E. Katz, U. Lawrentz, J. Granstrom, E. Reichmanis, Investigation of solubility-field effect mobility orthogonality in substituted phenylene-thiophene co-oligomers, Chem. Mater. 19 (2007) 4676–4681. https://doi.org/10.1021/cm070330j.

[37] S. Hotta, Y. Ichino, Y. Yoshida, M. Yoshida, Spectroscopic features of thin films of thiophene/phenylene co-oligomers with vertical molecular alignment, J. Phys. Chem. B. 104 (2000) 10316–10320. https://doi.org/10.1021/jp002166s.

[38] H.H. Choi, K. Cho, C.D. Frisbie, H. Sirringhaus, V. Podzorov, Critical assessment of charge mobility extraction in FETs, Nat. Mater. 17 (2017) 2–7. https://doi.org/10.1038/nmat5035.

[39] Y. Xu, Y. Li, S. Li, F. Balestra, G. Ghibaudo, W. Li, Y.F. Lin, H. Sun, J. Wan, X.

Wang, Y. Guo, Y. Shi, Y.Y. Noh, Precise Extraction of Charge Carrier Mobility for Organic Transistors, Adv. Funct. Mater. 30 (2020) 1–23. https://doi.org/10.1002/adfm.201904508.

[40] C. Liu, Y. Xu, Y.Y. Noh, Contact engineering in organic field-effect transistors, Mater. Today. 18 (2015) 79–96. https://doi.org/10.1016/j.mattod.2014.08.037.

[41] H. Bronstein, C.B. Nielsen, B.C. Schroeder, I. McCulloch, The role of chemical design in the performance of organic semiconductors, Nat. Rev. Chem. 4 (2020) 66–77. https://doi.org/10.1038/s41570-019-0152-9.

[42] A. Giovannitti, D.T. Sbircea, S. Inal, C.B. Nielsen, E. Bandiello, D.A. Hanifi, M. Sessolo, G.G. Malliaras, I. McCulloch, J. Rivnay, Controlling the mode of operation of organic transistors through side-chain engineering, Proc. Natl. Acad. Sci. U. S. A. 113 (2016) 12017–12022. https://doi.org/10.1073/pnas.1608780113.

[43] J. Liu, L. Qiu, G. Portale, M. Koopmans, G. ten Brink, J.C. Hummelen, L.J.A. Koster, N-Type Organic Thermoelectrics: Improved Power Factor by Tailoring Host–Dopant Miscibility, Adv. Mater. 29 (2017). https://doi.org/10.1002/adma.201701641.

[44] J. Liu, L. Qiu, R. Alessandri, X. Qiu, G. Portale, J.J. Dong, W. Talsma, G. Ye, A.A. Sengrian, P.C.T. Souza, M.A. Loi, R.C. Chiechi, S.J. Marrink, J.C. Hummelen, L.J.A. Koster, Enhancing Molecular n-Type Doping of Donor–Acceptor Copolymers by Tailoring Side Chains, Adv. Mater. 30 (2018) 1–9. https://doi.org/10.1002/adma.201704630.

[45] P. Durand, H. Zeng, T. Biskup, V. Vijayakumar, V. Untilova, C. Kiefer, B. Heinrich, L. Herrmann, M. Brinkmann, N. Leclerc, Single Ether-Based Side Chains in Conjugated Polymers: Toward Power Factors of 2.9 mW m−1 K−2, Adv. Energy Mater. 12 (2022) 2103049. https://doi.org/10.1002/aenm.202103049.

[46] X. Chen, Z. Zhang, Z. Ding, J. Liu, L. Wang, Diketopyrrolopyrrole-based Conjugated Polymers Bearing Branched Oligo(Ethylene Glycol) Side Chains for Photovoltaic Devices, Angew. Chemie - Int. Ed. 55 (2016) 10376–10380. https://doi.org/10.1002/anie.201602775.

[47] A. Armin, D.M. Stoltzfus, J.E. Donaghey, A.J. Clulow, R.C.R. Nagiri, P.L. Burn, I.R. Gentle, P. Meredith, Engineering dielectric constants in organic semiconductors, J. Mater. Chem. C. 5 (2017) 3736–3747. https://doi.org/10.1039/C7TC00893G.